Atmos. Chem. Phys. Discuss., 13, 27891–27936, 2013
www.atmos-chem-phys-discuss.net/13/27891/2013/
doi:10.5194/acpd-13-27891-2013

Atmospheric Chemistry and Physics Discussions

Observations of reactive nitrogen oxide fluxes by eddy covariance above two mid-latitude North American mixed hardwood forests

J. A. Geddes and J. G. Murphy

Department of Chemistry, University of Toronto, 80 St. George St., Toronto, ON M5S 3H6, Canada

Received: 22 September 2013 – Accepted: 14 October 2013 – Published: 29 October 2013

Correspondence to: J. G. Murphy (jmurphy@chem.utoronto.ca)

Published by Copernicus Publications on behalf of the European Geosciences Union.

Abstract

Significant knowledge gaps persist in the understanding of forest–atmosphere exchange of reactive nitrogen oxides, partly due to a lack of direct observations. Chemical transport models require representations of dry deposition over a variety of land surface types, and the role of canopy exchange of NO_x (= NO + NO_2) is highly uncertain. Biosphere–atmosphere exchange of NO_x and NO_y (= NO_x + HNO_3 + PANs + $RONO_2$ + pNO_3^- + ...) was measured by eddy covariance above a mixed hardwood forest in central Ontario (HFWR), and a mixed hardwood forest in northern lower Michigan (PROPHET) during the summers of 2011 and 2012 respectively. NO_x and NO_y mixing ratios were measured by a custom built two-channel analyzer based on chemiluminescence, with selective NO_2 conversion via LED photolysis and NO_y conversion via a hot molybdenum converter. Consideration of interferences from water and O_3, and random uncertainty of the calculated fluxes are discussed. NO_y flux observations were predominantly of deposition at both locations. The magnitude of deposition scaled with NO_y mixing ratios, resulting in campaign-average deposition velocities close to 0.6 cm s^{-1} at both locations. A period of highly polluted conditions (NO_y concentrations up to 18 ppb) showed distinctly different flux characteristics than the rest of the campaign. Integrated daily average NO_y flux was 0.14 mg (N) m^{-2} day^{-1} and 0.34 mg (N) m^{-2} day^{-1} at HFWR and PROPHET respectively. Concurrent wet deposition measurements were used to estimate the contributions of dry deposition to total reactive nitrogen oxide inputs, found to be 22 % and 40 % at HFWR and PROPHET, respectively.

1 Introduction

Emissions of NO_x from both anthropogenic and biogenic sources control tropospheric ozone production and the oxidizing capacity of the atmosphere through reactions involving hydrocarbons and OH radicals. The oxidation of NO_x to other species leads to particle formation and deposition of nitrogen, potentially far from sources where

ACPD
13, 27891–27936, 2013

ecosystems can be disrupted by the additional nutrients (Vitousek et al., 1997; Galloway et al., 2003).

Forests cover about 30 % of the Earth's land surface and influence climate through evapotranspiration, albedo effects, and carbon sequestration, but the net climate forcing from these is not well known (Bonan, 2008). Even less is understood about how nitrogen cycling and trace gas surface exchanges impact the atmospheric chemistry and carbon storage potential of forests. Nitrogen deposition from anthropogenic activities is postulated to have increased carbon uptake of forests across the Northern Hemisphere (Magnani et al., 2007; Thomas et al., 2010), but may also have detrimental effects at high levels (Vitousek et al., 1997). The recent rapid decline of NO_x emissions across most of North America and Europe motivated by air quality concerns is expected to have important consequences on the deposition of nitrogen to sensitive ecosystems. A decline in forest carbon uptake due to a weakening of the nitrogen fertilization effect would have implications for future climate predictions (Templer et al., 2012). It is therefore important to calculate accurate nitrogen deposition budgets in these changing environments.

Nitrogen is deposited out of the atmosphere by both wet and dry deposition. Nitrogen deposition budgets are generally calculated using two approaches: (1) by combining wet deposition observations across a network of precipitation sampling sites with dry deposition estimates inferred from a dry deposition model, forced by observed ambient concentrations at those sampling sites and observed meteorology; or (2) by fully modeling deposition using a chemical transport model driven by meteorology and emission estimates. Estimates of nitrogen deposition therefore depend on models with accurate surface and micrometeorological parameters, and sufficient observations (or adequate modeling) of all the relevent species. However, due to a lack of direct observations, dry deposition model parameterizations are based on limited datasets and unconfirmed assumptions (Wesely and Hicks, 2000; Flechard et al., 2011). Moreover, mixing ratio observations are sparse and are rarely available for all the necessary species, requiring

ACPD
13, 27891–27936, 2013

spatial interpolation and assumptions about the unknown contributions (Holland et al., 2005).

Using the former approach applied to the US and Europe, dry deposition was calculated to contribute 40–60 % of total NO_y deposition, although this only includes contributions from $HNO_{3(g)}$ and particulate nitrate in the US, and $HNO_{3(g)}$, particulate nitrate, and NO_2 in Europe (Holland et al., 2005). Given the potential contribution of species other than nitrate (and NO_2) to deposition, and frequent placement of deposition monitoring sites at remote locations, these are likely underestimates. At several locations across Canada, a deposition model that was applied to short term measurements of individual NO_y species estimated that dry deposition of non-nitrate species contributes equally or significantly more at every site (Zhang et al., 2009). At a site in North Carolina, nitrate was estimated not to be the dominant deposited species (Sparks et al., 2008). Similarly, at Harvard Forest, MA, nitric acid was estimated to contribute between 38–73 % of the total gaseous NO_y flux, with NO_x only partly compensating for the rest (Horii et al., 2006). Fully simulated deposition across the US using GEOS-Chem concluded that dry deposition contributes around 70 % of total NO_y deposition, with most significant contributions from $HNO_{3(g)}$, NO_2, isoprene nitrates, and peroxyacetyl nitrate, in that order (Zhang et al., 2012). The contribution of dry deposition to total deposition generally decreases with distance from source regions.

Exchange above forest canopies is affected by atmospheric inputs, surface emissions, and complex canopy interactions. NO_2 deposition can be offset by below canopy soil NO emissions that are rapidly converted to NO_2 (Wesely and Hicks, 2000). Uncertainties in the extent, and subsequent canopy losses (through chemistry and uptake), of primary soil NO emissions can confound modeling efforts (Ganzeveld et al., 2002). It is also unclear whether emission or deposition of NO_2 at leaf surfaces may be driven by a compensation point mechanism (Lerdau et al., 2000; Sparks et al., 2001; Chaparro-Suarez et al., 2011). Forests may therefore be sinks or sources of NO_x depending not only on proximity to anthropogenic sources and the strength of local soil emissions, but

ACPD
13, 27891–27936, 2013

a combination of other counteracting mechanisms which are not well characterized by observations.

Here we present results from two campaigns where mixing ratios and fluxes of NO_y were measured by eddy covariance at two comparable North American mixed forests located along the same latitude (45° N). While measurements of individual NO_y species were not made, simultaneous NO and NO_2 mixing ratios were measured. Shorter term eddy covariance measurements of NO_x flux were also performed at each site to help elucidate the role of the forests as net sinks or sources of NO_x. In this paper, the focus is on reporting the instrumental methods, summarizing the observations, and discussing the results in the context of quantifying a total oxidized nitrogen deposition budget (by incorporating observations from national wet deposition monitoring networks) and identifying the influence of atmospheric transport. Results are compared to other NO_y flux observations previously reported above forests across eastern North America.

2 Experimental

2.1 Sites

Observations were made from 20 July to 11 October 2011 at Haliburton Forest and Wildlife Reserve (HFWR, 45°17′11″ N, 78°32′19″ W), located in central Ontario, and from 24 July to 14 August 2012 at the University of Michigan Biological Station (UMBS, 45°33′32″ N, 84°42′52″ W), located in northern Michigan. Both forests are characterized as mixed, marking the transition between deciduous forests to the south, and the coniferous forests to the north.

HFWR is privately owned land managed under selection system silviculture resulting in a mixed age canopy, with last harvesting near the tower site in 1997. The dominant species is sugar maple, with contributions from American Beech, Yellow Birch, eastern hemlock and eastern white pine. Measurements were made from the top of a 32 m tower, where the average canopy is 20–25 m high. UMBS is located approx-

ACPD
13, 27891–27936, 2013

imately 500 km directly to the west of HFWR. Measurements were made from the 30 m tall Program for Research on Oxidants: Photochemistry, Emissions and Transport (PROPHET, see Carroll et al., 2001) tower. The site is a secondary successional forest last disturbed by fire in 1923, with a mean canopy height of around 22 m. The dominant species here are bigtooth aspen and trembling aspen, with contributions from red maple and sugar maple, red oak, birch, beech, and white pine. The PROPHET tower is situated about 100 m to the south of an established AmeriFlux tower (Schmid et al., 2003).

The location of both sites is shown in Fig. 1.

2.2 Mixing ratios of NO, NO_2, NO_y, and O_3

Nitrogen oxides were measured by a custom-built dual channel chemiluminescence instrument from Air Quality Design Inc. (www.airqualitydesign.com). This instrument is similar to the NO_x instruments used in Lee et al. (2009) and Reidmiller et al. (2010) in that NO_2 conversion is based on a blue LED converter documented by Buhr (2007). NO_y conversion is achieved by passing the sample flow through a hot molybdenum oxide converter (MoC). Chemiluminescence is measured in 200 mL reaction chambers that are each kept at a pressure of 5.5 torr. The instrument has a detachable inlet component containing the converters in order reduce sampling losses of NO_y species. This inlet is connected to the calibration and detection systems by a weather-proof umbilical of approximately 40 m, which houses sampling lines, calibration input lines, ethernet cables, and power lines. The inlet was designed to be operated in two modes: (1) continuous NO_x-NO mode, where Channel 1 continuously samples NO_x by leaving the NO_2 converter on, while Channel 2 continuously samples NO by bypassing the MoC; and (2) alternating NO/NO_x – continuous NO_y mode, where Channel 1 alternates between NO and NO_x by switching the NO_2 converter on and off, while Channel 2 continuously samples NO_y through the MoC. No filtering for particles as components of NO_y was used (although a filter is located immediately following the MoC converter to avoid possible debris contacting the mass flow controllers).

ACPD
13, 27891–27936, 2013

Measurements were conducted on a 30 min cycle, with 30 s of dark count measurements (see below) for background corrections followed by 29.5 min of ambient sampling. Calibrations were performed every 5–7 h during the campaigns, by standard addition of NO over ambient air. For the HFWR campaign, the NO standard used was a BOC- Linde cylinder of 5 ppm NO (±10 %) in N_2. For the UMBS campaign, the standard used was a cylinder of 5.17 ppm NO (±5 %) in N_2. Dilution flow into the sample air was controlled by a Pneucleus mass flow controller with a trim pot that was adjusted to either 5.30 sccm or 7.05 sccm. NO_2 conversion efficiency of the LED converter and the MoC could be tested throughout the campaign by titrating approximately half of the calibration NO with O_3. Controlled in-lab conversion efficiency experiments before and after the campaign were also performed. In addition to the uncertainty in the standards, uncertainty in the mixing ratios due to random error (3σ) during calibrations was less than 5 % for NO and NO_y during the HFWR and PROPHET campaigns, but 19.2 % and 11.1 % for NO_2 respectively due to conversion efficiency calculations. The NO_y conversion efficiency for NO_2 and HNO_3 were tested before and after the campaigns, and were within 10 % of unity.

Throughout the campaigns, the inlet was used most in Mode 2, allowing for simultaneous measurements of NO and NO_2 mixing ratios (by interpolation), and continuous NO_y mixing ratios. Since NO_y observations went uninterrupted for 29.5 min at a time, eddy covariance NO_y fluxes could be calculated. When operating in Mode 1 (for 3 non-continuous weeks and 5 consecutive days at HFWR and PROPHET respectively), eddy covariance NO_x fluxes could be calculated. Consistency between the two channels could be tested throughout the campaigns when Channel 2 bypassed the MoC (Mode 1), and the NO_2 converter in channel 1 was left off for first 30 s of sampling after dark counts. This allowed for simultaneous detection of NO in both channels once every 30 min. From these tests, NO mixing ratios in channel 1 and channel 2 were indistinguishable (e.g. at HFWR, slope of least orthogonal distance regression of 0.975 ± 0.003, Pearson $R^2 = 0.995$), within the random error of the individual calibrations (< 3.5 % on average).

ACPD
13, 27891–27936, 2013

The instrument ran with data collection at 5 Hz. The detection limits (signal-to-noise ratio of 3) for NO, NO_2, and NO_y were around 30, 120, and 30 ppt s^{-1} respectively. Backgrounds and chemical interferences ("dark counts") were determined by mixing the sample air with O_3 upstream of the main reactor. These counts were subtracted from the main chamber signal at other times (based on linear interpolation between tests). Zero air from a Sabio 1001P compressed air generator was also used to test for artefacts, however the response from this was occasionally above ambient signals at both HFWR and UMBS, and was therefore not subtracted from the signal. At PROPHET, after correcting for dark counts, night time NO mixing ratios were usually below the detection limit, so no further corrections were applied. At HFWR, artefacts not accounted for in the dark counts were determined by subtracting the minimum observed NO over each night (mean $\pm 1\sigma = 59$ ppt $\pm$ 50 ppt), interpolated between each day. This assumes that deviations from the expected value of close to zero at night were due to the instrument, and incorrectly account for artefacts if the interferences have a diurnal profile. Similar procedures have been applied elsewhere (e.g. Lee et al., 2009).

At HFWR, a generator was required to power the instruments. This resulted in observable spikes in the NO_x and NO_y timeseries. In most cases, these times were easily identified manually and removed in post-processing. After initial manual identification, other spikes (whether due to the generator or not) were identified by a technique based on the median of absolute deviation about the median, performed on the double-differenced time series with a 7 day running window. This method has been used previously for identifying spikes in half-hour eddy covariance fluxes (Papale et al., 2006), but was also deemed to perform well for this purpose as opposed to filtering based on a running standard deviation. From the whole campaign, approximately 30 % of the data was removed.

Ozone was monitored during both campaigns by a commercial O_3 UV analyzer (Thermo model 49C), sampled every 10 s (precision of 1 ppb).

ACPD
13, 27891–27936, 2013

2.3 Eddy covariance fluxes of NO_x and NO_y

The eddy covariance flux of a chemical species crossing a horizontal plane at instrument height is calculated as the covariance between instantaneous deviations of wind speed and the species mixing ratio relative to an averaging period:

$$F_c = \frac{1}{n}\sum_{i=1}^{n}[(w_i - \overline{w})\cdot(c_i - \overline{c})] \quad (1)$$

where n is the number of points per averaging period, w is vertical wind speed, and c is the mixing ratio of the species of interest (the subscript i represents the instantaneous measurement, while the overbar denotes the mean for the averaging period). In the present study, fluxes are calculated for half hour averaging periods, and the mean vertical wind was minimized by applying the planar fit correction approach presented by Wilczak et al. (2001).

Analog signals from the instrument were directed to a CR3000 datalogger that was collecting the wind measurements from the sonic anemometer at 10 Hz. For the purposes of flux calculations, the analog signal could be used to perfectly synchronize the observations from the instrument with the data from the sonic anemometer (the analog signals from the instrument collected by the datalogger were not used directly for the flux calculation since it was not possible to log important valve states (calibration times, zeros) due to a lack of analog outputs from the instrument). The data were re-synchronized in 5 to 7 day chunks and the instrument and datalogger clocks were found to drift approximately 3 to 4 s during this length of time. It was assumed that the lag-time calculation (see immediately below) corrected for this component of drift.

The intake line for NO_x and NO_y sampling was 60 cm away from the sonic anemometer. Sampling flow rate in each channel was 1.5 L min^{-1}, through tubing of 0.062″ inner wall diameter. The time lag between an observation of wind made by the sonic anemometer, and the NO_x or NO_y mixing ratios in that same parcel of air must be accounted for due to this sensor separation, in addition to transit time in the long sampling

ACPD
13, 27891–27936, 2013

lines of the NO_y instrument. This was performed by determining maximum correlation between w' and NO_y' in a lag correlation plot every half hour. Figure 2 shows an average of this calculation compared to the average lag plot for CO_2 which was also measured during the campaign by an open path infra-red gas analyzer for CO_2 fluxes.

For eddy covariance to be valid the assumption of stationary flow must be satisfied, and this can be tested for using the method proposed by Foken and Wichura (1996). In this approach, half hour covariances are compared to the mean of the covariances calculated in six consecutive 5 min windows within each half hour. Half hours when these two quantities differed by greater than 40 % were removed from the analysis. We do not apply any u_* filter to the reactive nitrogen oxide fluxes.

Corrections for flow distortion identified by integral turbulence statistics (e.g. σ_w/u_*) due to the influence of the tower required the removal of data from wind directions between 0–93° at HFWR. At this location, wind from this direction tends to represent unpolluted conditions and therefore removing this data introduces a possible selection bias. However, of the data left after other QAQC steps, only an additional 3–4 % of the data was removed. No such removal of data was required for the PROPHET dataset.

2.3.1 Flux interferences

The calculation of a scalar flux by eddy covariance can be affected by interferences from co-varying scalars such as temperature and water, if those scalars affect the density of air or the response of the instrument.

The "WPL" correction (Webb et al., 1980) accounts for the effect of temperature and water or air density fluctuations. In closed-path instruments and/or in cases when temperature is held constant, fluctuations in air temperature are unimportant, but Eq. (22) of Webb et al. (1980) shows how fluctuations in water may still cause errors:

$$F_c = \overline{\rho}[\overline{w'c'} + \{\overline{C}/(1-q)\}\overline{w'q'}] \quad (2)$$

where ρ is the density of moist air, C is the scalar (NO_y), and q is the specific humidity. The first term in the square parentheses represents the measured half-hour covariance

ACPD
13, 27891–27936, 2013

of vertical wind and mixing ratio, while the next term in the parentheses represents the correction that must be applied, which is a function of the average mixing ratio, specific humidity, and water vapour flux. In several previous examples of reactive nitrogen oxide fluxes by eddy covariance, this correction is ignored by finding or assuming that it is negligible (Munger et al., 1996; Farmer et al., 2006; Turnipseed et al., 2006). Colocated latent heat fluxes were measured at HFWR during the campaign, and at a flux tower close to PROPHET during that campaign, so estimates of this correction term could be calculated. Because water vapour was not measured in the closed-path reaction cell, we made this estimate by assuming there is no dampening of the water vapour flux (measured by an open path sensor) within our instrument tubing. Thus, the estimate of this correction term must be an overestimate of the true correction required. Using Eq. (22) of Webb et al. (1980), we found that for a large majority of the data, the correction term would be less than 1 % of the measured covariance. This term becomes largest during the daytime when the evapotranspiration of water is highest (approaching 0.18 and 0.15 ppt m s^{-1} on average at PROPHET and HFWR respectively). When the correction term approaches 10 %, the fluxes were almost always below the detection limit (discussed below).

As pointed out by Ammann et al. (2012), the chemiluminescent reaction on which the detection of reactive nitrogen oxides is based is sensitive to water vapour, which acts as a quencher and could therefore also lead to an artificial component of the flux. Previous lab studies with the instrument used here showed a linear reduction in sensitivity of about 0.6 % and 0.7 % per g m^{-3} of water vapour increase in Channel 1 and Channel 2 respectively. Using the H_2O flux data again an estimate of the correction term can be made. Like the WPL correction, this estimated correction term reaches an absolute maximum during the daytime (0.79 and 0.67 ppt m s^{-1} on average), about 4–5 times larger than the estimated WPL correction term (consistent with what was found by Ammann et al., 2012). It can therefore become important (> 5 % of the calculated flux); if only the fluxes above the detection limit are considered, about 12 % of the data have correction terms greater than 5 %.

ACPD
13, 27891–27936, 2013

To the above interferences we add the consideration of the NO + O_3 back reaction within the sampling lines, which affects the amount of NO that is detected in the reaction chambers. While average mixing ratios can be corrected by using colocated O_3 mixing ratio observations, high frequency fluctuations (> 0.1 Hz) in ozone, which may covary with the fluxes of reactive nitrogen oxides, could not be measured by the ozone instrument used in this study. A rough estimate of this term is therefore calculated given previously measured O_3 deposition observations at PROPHET and at a similar site, Harvard Forest. Calibrations throughout the campaigns could be used to determine the sensitivity of the NO + O_3 back reaction to ambient O_3 mixing ratios since calibrations were performed as standard additions over ambient air. Again, the absolute magnitude of this correction term reaches a maximum during the day time, that we expect would co-occur with maxima in H_2O fluxes due to the fact that O_3 fluxes are similarly controlled by stomatal opening (Hogg, 2007). However, the sign of this correction term is opposite to the water correction term. While both O_3 and H_2O affect the response of NO in a similar way (decreasing "sensitivity" with increasing concentrations), the flux of O_3 is opposite to the flux of water. Given an average O_3 deposition flux of about 40 $\mu mol\,m^{-2}\,h^{-1}$ (Munger et al., 1996; Hogg, 2007), the correction term is estimated to be 0.41 $ppt\,m\,s^{-1}$ 0.65 $ppt\,m\,s^{-1}$ for measurements of NO_x and NO_y fluxes respectively (the sensitivity to the reaction of NO + O_3 in the tubing changes when the heated molybdenum converter in used).

These considerations illustrate how, beyond the instrumental challenges of measuring reactive nitrogen oxide fluxes, the interpretation of their results remains even more challenging. The average diurnal pattern of the estimated correction terms for the PROPHET campaign is shown in Fig. 3. Since actual correction terms could not be calculated because water is not measured within the reaction chamber and fast enough ozone measurements could not be made, we do not apply any correction to the measurements, arguing that (1) the estimated correction terms are an overestimate because we have calculated them assuming no dampening within the sample tubing and (2) that the water and ozone correction terms are most important at the same time

ACPD
13, 27891–27936, 2013

of day, and have shown to be of the similar magnitudes but opposite signs. For fluxes of NO_y, this means that the error caused by an artificial component of the flux due to water and ozone must for most of the time be less than 10 %, and in many cases likely smaller than 5 %.

2.3.2 Random uncertainty

Random uncertainty for the half hour fluxes were estimated using on two approaches. First, for both campaigns, a technique based on a minimum lag-correlation calculation was used. For each half hour, the maximum covariance between the scalar of interest and vertical wind is calculated to correct for time lag effects (see above). This measurement is assumed to be the "true" covariance for that half hour. Then, a "zero" covariance is calculated by introducing a constant delay to the scalar wave and re-calculating the covariance. Analyses were done for lags of 20 s and 60 s. The assumption here is that at these time points, "true" covariance between w' and the scalar is minimized (illustrated in the lag correlation plot of Fig. 2) and can therefore be used as an estimate of zero flux. Any covariance that results is therefore assumed to be due to instrument noise and other error. If the error is random, an average over multiple observations should be close to zero, and the standard deviation represents an estimate of "noise" in flux observations. To calculate an appropriate uncertainty for every half hour observation, the "zero" flux measurements were grouped into bins of equal numbers based on the magnitude of true covariance, and the standard deviation of that group is used as an estimate of the uncertainty. Due to signal dampening in the sensor lines and atmospheric effects, the true timing of the minimum covariance may change, and signal "leakage" may occur causing this calculation to be an overestimate of the uncertainty.

A second approach was tested during during the HFWR campaign, where 30 min of signal with just zero air was used to calculate covariances at each half hour with the measured vertical wind. This method, described in Billesbach (2011), and also applied to nitrogen oxide fluxes by Farmer and Cohen (2008), has been referred to as a "minimum detectable fluxes" approach. Observations were again grouped into bins

ACPD
13, 27891–27936, 2013

based on the magnitude of the true covariance. While this approach avoids the signal "leakage" issue, its limitation is the assumption that uncertainties are independent of mixing ratio observations. We therefore expect uncertainties calculated by this method to be an underestimate.

The results of the uncertainty analysis are shown in Fig. 4 for NO_y covariance and using the artifical lag of 60 s. With the lag-time approach, the absolute precision of the observations is directly related to the magnitude of the true covariance. So, maximum covariances around $-1\,\mathrm{ppt\,m\,s^{-1}}$ have an uncertainty of $0.5\,\mathrm{ppt\,m\,s^{-1}}$, while maximum covariances around $-30\,\mathrm{ppt\,m\,s^{-1}}$ have an uncertainty of $5\,\mathrm{ppt\,m\,s^{-1}}$ (the observations are assigned a value based on $\pm 1\sigma$) at both PROPHET and HFWR. Here, observations are considered above the "detection limit" when they are greater than three times the uncertainty (i.e. 3σ). At PROPHET and HFWR, this is true of observations of deposition greater than about $3\,\mathrm{ppt\,m\,s^{-1}}$. Observations of emissions during both campaigns all had a 3σ uncertainty around 100 %. A similar analysis for the NO and NO_2 fluxes showed that deposition of NO greater than $1\,\mathrm{ppt\,m\,s^{-1}}$ were above the detection limit, but all observed emissions of NO and all observed NO_2 fluxes were below the detection limit. Consistent results were found using the lag time of 20 s.

Applying the zero air approach at Haliburton yields slightly different results (shown in Fig. 4). As expected, the absolute precision is less a function of the true covariance. This method calculates a worse precision than the time-lag approach for the lowest observations ($\pm 0.6\,\mathrm{ppt\,m\,s^{-1}}$ for covariances close to zero) and better precision at the highest observations ($\pm 1\,\mathrm{ppt\,m\,s^{-1}}$ for observations around $30\,\mathrm{ppt\,m\,s^{-1}}$). The true uncertainty in the observations is likely somewhere in between these estimates.

2.3.3 Cospectral analysis

Cospectral analysis is often performed to investigate attenuation of high frequency components of measured fluxes. In our case, the most significant sources of high frequency attenuation are expected to be sampling frequency limitations (governed by flow rate) and attenuation of high frequency variations in the tubing (governed by tran-

ACPD
13, 27891–27936, 2013

sit time and flow characteristics). Attenuation due to sensor separation between the inlet and sonic anemometer is assumed to be corrected for by the lag time correction. Lab tests performed before the field campaigns (by alternating ambient sampling with zero air overflow at the inlet) demonstrated the instrument had a time response governed by an exponential time constant of approximately 1 s (data not shown).

Attenuation due to tubing effects has been proposed to be accounted for by modeling a transfer function, $T_t(n)$, according to Eq. (1) in Suyker and Verma (1993), which would be applied to an ideal cospectrum:

$$T_t(n) = \exp\left[-4\pi^2 n^2 \Lambda L a u_t^{-2}\right] \quad (3)$$

where n is frequency (Hz), Λ is a tube attenuation coefficient, L is the tube length (40 m), a is the tube radius, and u_t is the mean flow velocity in the tube. The form of the tube attenuation coefficient depends on whether tube flow is turbulent or laminar. An estimate of the Reynolds number for flow in the instrument suggests flow is laminar, so that the tube attenuation coefficient is governed by Eq. (3) in Suyker and Verma (1993):

$$\Lambda = 0.0104 v Re D^{-1} \quad (4)$$

where v is the kinematic viscosity of air, Re is the Reynolds number, and D is the molecular diffusivity of the gas (here using NO). For the purposes of this calculation, it was assumed that pressure in the tubing decreased linearly from ambient conditions at inlet to the total 11 torr at the reaction chambers.

For an ideal cospectrum, we use the $w'T_s'$ cospectrum, were T_s' is the temperature measured by the sonic anemometer. If modeled correctly, the attenuated cospectrum should agree with the observed $w'NO_y'$ cospectral shape. To investigate this, Fig. 5a shows an average normalized cospectrum of $w'NO_y'$ from 28 July to 30 July during the HFWR campaign, and Fig. 5b shows the average normalized cospectrum of $w'NO_y'$ from 2 August to 4 August during the PROPHET campaign. These are compared with the cospectra of $w'T_s'$ for the same period, and their attenuated cospectra using the

ACPD
13, 27891–27936, 2013

transfer function of Eq. (3). The empirical curve from Kaimal et al. (1972) for neutral stratification is shown for the sake of comparing the shape of the curves.

As shown in Fig. 5, the slopes of the cospectra of $w'NO_y'$ from the peak maximum to around 0.3 Hz compare well with the slopes of the $w'T_s'$ cospectra. However, beyond this frequency, instead of observing the expected decrease in spectral power according to tube attenuation for $w'NO_y'$, there is a slight increase in power before it decreases sharply. This behaviour could be expected in instruments with a large amount of noise in the high frequency. If the noise is truly random, there should not be significant covariance with fluctuations in vertical wind, however this has been observed in other situations (e.g. methane fluxes reported in Querino et al., 2011; Smeets et al., 2009). Therefore, given the evidence from Fig. 5 that the spectral shape beyond peak frequencies are similar for $w'NO_y'$ and $w'T_s'$, we apply a correction based on cospectral similarity instead of using the tube attenuation transfer function. This correction is applied by comparing the integrating the area under the non-normalized cospectra of $w'NO_y'$ up to 0.3 Hz with the ratio of the total covariance of $w'T_s'$ to the integrated area under the non-normalized cospectra of $w'T_s'$ up to 0.3 Hz:

$$w'NO'_{y,\mathrm{ideal}} = \int_0^{0.3\,\mathrm{Hz}} \mathrm{Co}_{w'NO_y'} \frac{w'T'_{s,\mathrm{meas}}}{\int_0^{0.3\,\mathrm{Hz}} \mathrm{Co}_{w'T_s'}} \tag{5}$$

where $w'NO'_{y,\mathrm{ideal}}$ is the corrected covariance for flux calculations. On average, the integrated area from 0 to 0.3 Hz of $\mathrm{Co}(w'T_s')$ was greater than 95 % of the total area during the middle of the afternoon, and slightly higher than 90 % of the total area around midnight.

ACPD
13, 27891–27936, 2013

3 Observations

3.1 Mixing ratios of NO_x, NO_y, and O_3

The campaign average mixing ratios of NO, NO_2, and NO_y are shown as a fuction of time of day in Fig. 6. NO and NO_2 mixing ratios at PROPHET and HFWR displayed the expected diurnal patterns driven by photochemistry. Night time NO mixing ratios were close to zero, while NO_2 built up to a median of around 500 ppt at both PROPHET and HFWR. At PROPHET, NO_2 levels continued to rise during the early morning hours to a median of close to 1000 ppt. This latter observation has been seen previously at PROPHET and has been discussed elsewhere (Alaghmand et al., 2011; Seok et al., 2013). During the later morning hours, photolysis of NO_2 at both locations resulted in an increase in NO mixing ratios until an approximately steady state is reached in the afternoon. Mid-day NO and NO_2 mixing ratios were 60 ppt and 250 ppt for PROPHET and 150 ppt and 360 ppt at HFWR respectively. Average NO_y appears to exhibit different diurnal patterns at each location. During PROPHET, NO_y levels peak in the early morning (median of 1600 ppt), then are steady throughout the afternoon and night time (median around 1000 ppt). At HFWR, median NO_y reaches a maximum (approaching 1500 ppt) in the late morning that persists throughout the afternoon, until the evening when levels stabilize around 1000 ppt for the rest of the night. Ozone mixing ratios at both locations rapidly decreased during the night to a minimum around 07:00 Local Time (LT) of 21–23 ppb on average, and increased during the day to a maximum around 16:00 LT of 32 ppb on average.

3.2 NO_y fluxes

NO_y flux observations at both PROPHET ($N = 348$) and HFWR ($N = 829$) were predominantly of deposition, while the random uncertainty of emissions that were observed was often greater than 100 % (i.e., error may account for the majority of these instances). Deposition was higher at PROPHET than at HFWR, both in terms of maxi-

ACPD
13, 27891–27936, 2013

mum observed values and in terms of long-term average. At HFWR, 73.6 % of the observed fluxes were negative (mean $\pm 1\sigma = -3.1 \pm 8.5$ ppt m s^{-1}). At PROPHET, 81.9 % of the observed fluxes were negative (mean $\pm 1\sigma = -7.4 \pm 13.3$ ppt m s^{-1}). Ten-day segments of the half-hour NO_y flux timeseries from PROPHET and HFWR are shown in Fig. 7, with the corresponding half-hour average NO_x and NO_y mixing ratios. In general, fluxes scaled with NO_y mixing ratios, with higher deposition measured at higher mixing ratios. The scaling of deposition with mixing ratio means that infrequent periods of high NO_y mixing ratios can contribute disproportionately to long-term deposition (similar to the episodic nature of wet deposition). Episodes of high concentrations were usually associated with flow from particular regions (the contribution of polluted flow from upwind source areas is investigated in more detail below).

An unusual event occured at HFWR from 7–9 October 2011 during which very high NO_y mixing ratios (> 18 ppb, > 6 ppb, and > 5 ppb on the 7, 8, and 9 of October respectively) were observed along with high O_3 mixing ratios (above 60 ppb on each day). Air quality monitoring data from across the region suggests (http://www.airqualityontario.com) this was an event characterized by high O_3 and $PM_{2.5}$ probably experienced by a large portion of central Ontario, extending at least as far as 140 km to the northwest of HFWR, and possibly as far as the Toronto area 200 km to the south. Data from the National Geophysical Data Center show the timing of this event coincided with large smoke plumes that were observed over north-central Ontario and northern Quebec for several days (http://maps.ngdc.noaa.gov/viewers/firedetects). In light of the high $PM_{2.5}$ that was recorded at an air quality monitoring site 20 km west of the HFWR tower (hourly average concentrations greater than 20 µg m^{-3}, when they were typically less than 6 µg m^{-3} in the preceding and following weeks), we take this as evidence that the source of the high concentrations could have been forest fire. The NO_y fluxes during this time displayed a clearly different pattern compared to the rest of the campaign, and for this reason is discussed separately and excluded from the analysis of the rest of the campaign as described below.

ACPD
13, 27891–27936, 2013

NO_y fluxes as a function of time-of-day from PROPHET and HFWR are shown in Fig. 8. Hourly averages are also plotted (observations were grouped into hourly bins instead of half-hour bins to increase the number of data points), and the diurnal traces of u_* and Monin-Obhukov z L^{-1} are also shown in Fig. 8. Fluxes at both sites exhibited diurnal patterns, with higher deposition during the daytime and fluxes close to zero at night time. Occasionally, observations of emissions were observed in the afternoons, and there were several examples of high deposition throughout the night during both campaigns. Deposition peaked at PROPHET between 11:00 LT and 16:00 LT, exceeding 15 ppt m s^{-1} on average. Previous NO_y flux measurements from PROPHET using a similar method during August 2005 report a lower peak in average day time deposition of around 10 ppt m s^{-1} (Hogg, 2007), although occurring at a similar time of day. Deposition at HFWR peaked earlier in the day and at about half the magnitude compared to PROPHET (about 7 ppt m s^{-1}). While average deposition at PROPHET seems to follow the pattern in u_*, deposition at HFWR peaks earlier than the maximum u_*.

On the other hand, the unusual behaviour of the 7–9 October event at HFWR is illustrated in Fig. 9, which shows a diurnal pattern that is opposite to the rest of the campaign. High rates of deposition are recorded during the night, and high rates of emission or recorded during the day. It appears that under these highly polluted conditions, the forest is not a permanent sink of the reactive nitrogen that was deposited into the canopy at night, but rather it expelled some of this material during the daytime when the atmospheric mixing ratios of NO_y were lower.

NO_y fluxes correlated with NO_y mixing ratios. Linear slopes based on regression of the half-hourly data were significant and very similar between the two locations (0.58 ± 0.02 and 0.57 ± 0.06 cm s^{-1} at PROPHET and HFWR respectively). These slopes represent campaign-average NO_y deposition velocity, and are within the range observed during the summertime at Harvard Forest (Munger et al., 1996). However, at any given time this parameter is expected to be controlled by atmospheric conditions and, for example, the ratio of NO_x to NO_y.

ACPD
13, 27891–27936, 2013

Since the NO_y flux observations at both locations were discontinuous, gap-filling such a short data set is not feasible. Net daily NO_y exchange at PROPHET and HFWR during the campaign was therefore estimated by integrating the mean diurnal traces. At PROPHET, net deposition of 0.34 mg (N) m^{-2} day^{-1} was calculated. At HFWR, the average for the majority of the campaign (Fig. 8) calculates a net daily deposition of 0.14 mg (N) m^{-2} day^{-1}. The net daily deposition from 7 October to 10 October (Fig. 9) was 0.22 mg (N) m^{-2} day^{-1} but this event only nominally affects the campaign average for HFWR, which remains at approximately 0.14 mg (N) m^{-2} day^{-1}. These are of the same order of magnitude as the handful of previously reported summertime NO_y fluxes from other forest sites across North America (Sparks et al., 2008; Munger et al., 1998; Hogg, 2007). Table 1 compares mean results from previous NO_y eddy covariance flux studies in mg (N) m^{-2} day^{-1}, with a focus on summertime observations. Results from the present PROPHET campaign lie between previously observed values, while results from HFWR are on the low end. A detailed comparison of these results, however, is not straightforward due to the span of over two decades across the observations that have seen strong declines in NO_x emissions in these regions of North America, and the short duration (a few weeks) of most of the campaigns that cannot accurately capture long-term averages.

3.3 NO_x fluxes

Eddy covariance NO and NO_2 flux observations were made for several days at PROPHET, and for several weeks at HFWR (see Sect. 2.2). Uncertainties in individual half-hour NO and NO_2 flux observations were around 100 % most of the time, indicating that the precision of this instrument was not adequate to make reliable observations of NO_x flux at these sites. We restrict our interpretation of this data to the resulting diurnal average profiles in order to at least reduce the effects of random variability by grouping observations from the same time of day.

ACPD
13, 27891–27936, 2013

The diurnal plots are shown in Fig. 10. Generally, mean night time observations were close to zero and impossible to detect, while during the day time, mean fluxes outside the random variability could be detected. Fluxes of NO and NO_2 largely cancel each other out. The diurnal profiles observed here show apparent emission of NO_2 (median peak of $-4.8\,\mathrm{ppt\,m\,s^{-1}}$ and $-2.6\,\mathrm{ppt\,m\,s^{-1}}$ at PROPHET and HFWR, respectively) and apparent deposition of NO (mean peak of $+4.0\,\mathrm{ppt\,m\,s^{-1}}$ and $+2.1\,\mathrm{ppt\,m\,s^{-1}}$ at PROPHET and HFWR, respectively) during the day time.

4 Discussion

4.1 Influence of transport

As a basic measure of the influence of transport, we grouped NO_y flux observations by wind direction at both locations ("north", "southwest", and "southeast"). At HFWR, the "north" category only included observations from 270 to 360°, due to the influence of the tower from 0 to 93°. At PROPHET, "north" included all observations between 270 and 90°. The results are shown in Fig. 11.

The data from both locations reveal a strong influence of wind direction on the magnitude of deposition. At PROPHET, flow from the southwest (from the direction of the Milwaukee and Chicago areas across Lake Michigan) is associated with the highest deposition (mean = $-14.6\,\mathrm{ppt\,m\,s^{-1}}$). Deposition is also enhanced when flow from the southeast (from the direction of Detroit, Cleveland, and populated regions in southwestern Ontario) is observed (mean = $-5.8\,\mathrm{ppt\,m\,s^{-1}}$). Observations from the north are still of deposition on average (mean = $-2.5\,\mathrm{ppt\,m\,s^{-1}}$), although with less skew towards high values. At HFWR, deposition looks approximately normally distributed around zero when flow is coming from the north (mean = $-0.3\,\mathrm{ppt\,m\,s^{-1}}$), whereas deposition is enhanced when wind comes from the south (from the direction of the greater Toronto area in southern Ontario), and skewed towards high values (mean = $-4.2\,\mathrm{ppt\,m\,s^{-1}}$ and $-3.0\,\mathrm{ppt\,m\,s^{-1}}$ for the southwest and southeast respectively).

ACPD
13, 27891–27936, 2013

PROPHET and HFWR represent receptor locations where the amount of pollution received is dependent on transport conditions and source regions. It is not surprising, therefore, that there is a clear association of deposition with wind direction; NO_y deposition has already been seen to be driven by atmospheric mixing ratios. However, these observations represent some of the first directly measured evidence of this effect on the dry deposition of reactive nitrogen oxides at mid-latitude forests in North America since the long-term Harvard Forest results from 15 yr ago (Munger et al., 1996), and may therefore be valuable for comparisons with model output. Despite strong reductions over the last decade in anthropogenic reactive nitrogen oxide sources, transport of NO_y still contributes significantly to nitrogen deposition at these locations. Since the deposition in these regions can be very low or very high depending on meteorological conditions, they provide a good dynamic range for validation. In the future, more intensive campaigns at these locations with speciated measurements of NO_y should elucidate how source region impacts the chemical components that are being deposited, providing further constraints on modeled deposition.

4.2 Total deposition budget of reactive nitrogen oxides

It is desirable to assess the contribution of wet and dry deposition to total reactive nitrogen oxide deposition. As described in the introduction, usually these budgets rely heavily on models and are associated with sometimes unquantifiable uncertainties (Holland et al., 2005). While wet deposition is easily measured directly using precipitation sampling networks, dry deposition is estimated using deposition models with ambient concentrations as inputs. The contributions of wet vs. dry deposition not only depends on meteorological considerations, but also on the proximity to sources.

Deposition budgets at individual sites where dry and wet deposition were both measured directly (instead of being inferred) are rare, and even more rare when contributions from individual NO_y species are measured simultaneously. Munger et al. (1998) describe the budget for Harvard Forest using NO_y eddy covariance flux data collected from 1990–1996, and show that on an annual basis, dry deposition contributes 34 %

ACPD
13, 27891–27936, 2013

of total NO_y inputs; the same paper summarizes data collected during the summer of 1990 over a black spruce woodland in northern Quebec which shows that contributions of dry deposition is roughly the same. Sparks et al. (2008) report a much higher dry NO_y deposition contribution to total nitrate on an annual basis of around 60 % above a North Carolina pine plantation. Other studies using eddy covariance have applied novel instruments to directly determine the contribution of individual species over short-term (several months or less) intensive field campaigns at a number of sites across North America (Horii et al., 2004; Turnipseed et al., 2006; Farmer and Cohen, 2008; Wolfe et al., 2009; Min et al., 2012; Zhang et al., 2012). Gradient methods above forest canopies have also been used to determine the contributions of certain species to NO_y deposition or emission budgets (Sievering et al., 2001; Pryor et al., 2002; Neirynck et al., 2007; Wolff et al., 2010).

For the present analysis, wet deposition observations that were made over the concurrent summer months were scaled down to an average daily flux for comparison with the average daily NO_y flux measured during the two campaigns.

4.2.1 PROPHET

The National Atmospheric Deposition Program includes a monitoring station at Douglas Lake, within the UMBS property where the PROPHET tower is also located. Here, the concentration of nitrate in precipitation is recorded, and can thus be used in a comparison with the dry deposition measured during the campaign. Data from July and August 2012 was accessed from http://nadp.sws.uiuc.edu/. Total nitrate deposited in precipitation from July to August was $0.15\,g\,(NO_3^{-1})\,m^{-2}$, or approximately $0.55\,mg\,(N)\,m^{-2}\,day^{-1}$ on average over July–August. The diurnally averaged NO_y flux observations provide an estimate of dry deposition of $0.34\,mg\,(N)\,m^{-2}\,day^{-1}$. This would suggest that during this summer period, dry deposition contributed just under 40 % of the N in total reactive nitrogen oxide deposition.

ACPD
13, 27891–27936, 2013

This is significantly higher than the estimates made for August 2005, where NO_y fluxes were measured by eddy covariance at PROPHET (Hogg, 2007). During that campaign, dry NO_y deposition only contributed on the order of 10 % of total NO_y deposition (Hogg, 2007). Although these measurements were made at very similar times of the year, the 2005 and the present 2012 campaign estimates are only based on three weeks of dry deposition measurements each, and are therefore subject to significant short-term variations in pollutant concentrations and meteorology, which may explain some of the discrepancy. Both wet and dry deposition can be highly episodic, with short-term periods contributing disproportionately to total deposition. This underscores the need for fairly long-term measurements if better constraints are to be placed on the overall nitrogen deposition budget. However, both campaigns agree that NO_x was not a significant component of depositing NO_y.

4.2.2 HFWR

While precipitation was not monitored in the direct vicinity of the tower at HFWR, the Canadian Air and Precipitation Monitoring program records nitrate in precipitation at three sites located in surrounding areas, with data available for 2011 (http://www.ec.gc.ca/rs-mn/). Here, total nitrate in precipitation from July to September was calculated. Here we consider Warsaw Caves (44°27′36″ N, 78°7′48″ W), located approximately 80 km south of HFWR, which had 0.24 g (NO_3^{-1}) m^{-2}; Sprucedale (45°25′12″ N, 79°29′24″ W), located approximately 80 km northeast of HFWR, which had 0.17 g (NO_3^{-1}) m^{-2}; and Chalk River (65°3′36″ N, 77°24′36″ W), located approximately 110 km northwest of HFWR, which had 0.17 g (NO_3^{-1}) m^{-2}. This puts relatively good bound on possible wet nitrate deposition at HFWR, located centrally in relation to these three sites. We will use an estimate of 0.2 g (NO_3^{-1}) m^{-2}, which results in wet deposition average of around 0.50 mg (N) m^{-2} day^{-1} over that time. Wet deposition measurements at the HFWR tower were collected manually during the summer and fall of 2009, which also result in an estimate of wet nitrate contributions on the order of

ACPD
13, 27891–27936, 2013

0.59 mg (N) m^{-2} day^{-1} (De Sousa, 2010), agreeing well with the other observations at different sites in the vicinity from 2011.

The diurnally averaged NO_y flux observations give an esimate of 0.14 mg (N) m^{-2} day^{-1}. This suggests that during this summer period, dry deposition contributed on the order of 22 % of total N in reactive nitrogen oxide deposition for the HFWR region. The estimate of the contributions of dry and wet deposition at HFWR is in reasonable agreement with previous modeling results, where the dry deposition of NO_y at eight locations across Canada contributed between 17 % and 60 % of the total reactive nitrogen oxide deposition (Zhang et al., 2009). At the two locations closest to HFWR, the contributions were 17 % and 24 % (modeled for Sprucedale and Chalk River, respectively).

4.3 Above canopy NO and NO_2 fluxes

The exchange of NO and NO_2 above forest canopies is not well understood. Above canopy NO_x fluxes by single point eddy covariance are difficult to interpret due to the comparable chemical and turbulent time scales (e.g. see Gao et al., 1991). This is exacerbated in the present work by the flux intereferences due to water and O_3, which have been estimated on average to approach 1 ppt m s^{-1} (albeit in opposite directions) during the daytime (see Fig. 3).

When observed directly, the NO and NO_2 fluxes showed that each tended to cancel the other out, suggesting NO_x may not make an important contribution to NO_y deposition at these forests. However, there were times during NO_y flux sampling that indicate otherwise. For example, at HFWR during the night of 24 August (see Fig. 7), the NO_x/NO_y ratios were high and large NO_y deposition was observed. NO_2 mixing ratios at this time were around 2700 ppt. Assuming the deposition velocity of NO_2 at this time could have been around 0.2 cm s^{-1} (Zhang et al., 2003), NO_2 alone could have accounted for around 60 % of the observed deposition. If we assumed the difference between NO_y and NO_x was made up entire of nitric acid, which could have a depo-

ACPD
13, 27891–27936, 2013

sition velocity close to 1.2 cm s^{-1} under the same conditions (Zhang et al., 2003), it would have approximately made up the rest of the observed deposition.

The apparent emission of NO_2 and deposition of NO observed at PROPHET and HFWR is likely an example of classic chemical flux divergence, where the true flux at the biosphere–atmosphere interface is not maintained at the measurement height (as has been predicted by models, e.g. Gao et al., 1993, and observed elsewhere, e.g. Horii et al., 2004). This results from fast chemistry below the canopy which depletes above-soil NO concentrations (from emission) and produces NO_2. Since the lifetime of NO_2 below the canopy can be longer than above the canopy due to the extinction of incoming radiation, significant vertical gradients in the NO/NO_2 ratio may develop and result in this chemical flux divergence. The observations of this flux-divergence phenomenon presented here are, as far as we know, some of only very few direct observations of this above forest canopies. Given that we have confirmed this behaviour at these sites, future measuremets that investigate flux divergence at HFWR and PROPHET would be beneficial since little experimental work is available on this topic.

Due to the flux divergence problem we have no constraint on the true magnitudes of NO emission fluxes from the soil and NO_2 deposition to the canopy. In addition to this problem, the detection of soil emissions by above-canopy flux observations also depends on the extent of canopy reduction processes and the relative importance of dry deposition to the canopy (since eddy covariance represents the net result of emission and deposition). Even the traditional assumption that NO_x (as the sum of NO and NO_2) is analogous to a conserved species, where the timescale of chemical conversion is much longer than turbulent timescales, is being challenged by evidence of within-canopy chemistry that may drive vertical chemical gradients (Min et al., 2013).

Typically, soil emissions are measured by chamber techniques directly above the soil surface. Such observations have informed attempts to parameterize soil NO_x emissions globally as a function of ecosystem type, soil temperature and wetness, fertilizer application, and precipitation patterns (e.g. Yienger and Levy, 1996; Steinkamp, 2011; Hud-

ACPD
13, 27891–27936, 2013

man, 2012). We are aware of very few published observations of NO emissions from North American forest soils (and none were performed during the present campaigns). Williams et al. (1988) reports mean soil NO emissions from a forest in Pennsylvania of 1.2 ng (N) m^{-2} s^{-1}; Williams and Fehsenfeld (1991) report mean soil NO emissions for a deciduous forest in Tennessee of 0.28 ng (N) m^{-2} s^{-1}; Munger et al. (1996) use profile measurements of NO_x to estimate maximum soil emissions from Harvard Forest of 3.5 ng (N) m^{-2} s^{-1}; Venterea et al. (2004) report mean soil NO emissions between 0.06 to 1.9 ng (N) m^{-2} s^{-1} for forests in Maine and Virginia. Unpublished data in previous years from the vicinity of the PROPHET tower indicated an average soil NO flux of around 0.7 ng (N) m^{-2} s^{-1}. From the available literature, if we consider a reasonable range in soil NO emissions at both locations of between 0.5 and 3 ng (N) m^{-2} s^{-1} and disregard for the moment any canopy and/or chemical losses, this would translate into emission contributions to the measured flux on the order of 0.8 to 5 ppt m s^{-1} NO_x.

These observations confirm the need for further understanding the role of soil NO_x emissions from forest systems, and the difficulty in constraining their magnitude. Soil NO_x emissions and interactions with forest canopies remain poorly modeled, limited by the lack of data for model verification and accuracy in the available observations (Fowler et al., 2009). In addition to better precision in above-canopy flux measurements, vertical gradient observations and/or ideally dedicated soil chamber measurements would be required in the future.

5 Conclusions

NO_y flux measurements above two comparable forests in North America have been presented. PROPHET and HFWR towers are both located within mixed forests that mark the transition between the deciduous and boreal forest, along 45° N. Observations from HFWR were made for nine weeks between late July and early October 2011, while observations at PROPHET were made for three weeks between late July and mid-August.

ACPD
13, 27891–27936, 2013

Results show that NO_y mixing ratios at PROPHET were slightly higher on average than at HFWR. Half hour NO_y fluxes were predominantly of deposition, and about twice as high at PROPHET than HFWR on average. In general, fluxes were on the same order of magnitude of previous observations elsewhere in North America. At both locations, we observed direct evidence of chemical divergence in NO and NO_2 fluxes, and are unable to constrain soil emissions or NO_2 deposition with these observations. Concurrent vertical profiles and soil chamber emission measurements would be beneficial in the future.

On an average daily basis, dry deposition of NO_y resulted in inputs of 0.34 and 0.14 mg (N) m^{-2} day^{-1} at PROPHET and HFWR respectively, contributing approximately 40 % and 22 % of total nitrate inputs from wet and dry deposition during the period of observations. Organizing the flux measurements by wind direction observed from the tower showed a significant influence of transport on deposition rates. Both sites experience elevated dry deposition when flow is coming from the south. As a result, high pollutant days have the potential to contribute disproportionately to overall deposition. Long-term measurements are therefore required to accurately assess the atmospheric nitrogen budget and reduce the influence of short-term variability on meteorology and transport conditions.

These observations should be useful in future model evaluation studies, and help bound the wet and dry deposition budgets in these regions. Further long-term measurements with speciated NO_y observations, and NO_x profile or soil chamber observations, would be desirable to provide even more detailed insight into model performance.

Acknowledgements. We gratefully acknowledge the support of collaborators from the HFWR-2011 and PROPHET-2012 field campaigns. Thanks to Sean Thomas, Jon Schurman, Alex Petroff, and Jon Wang (HFWR); Kevin McAvey, Steve Bertman, and Tim Starn (PROPHET). Thanks to Haliburton Forest and Wildlife Reserve Ltd for their support of our research at HFWR in 2011, and thanks to Mary Anne Carroll and Steve Bertman for the invitation to PROPHET in 2012. The authors also wish to thank Martin Buhr and David Tanner (Air Quality Design, Inc.) for their technical support. We also gratefully acknowledge the Natural Sciences and Engineering Research Council of Canada, and the Canada Foundation for Innovation, for funding.

ACPD
13, 27891–27936, 2013

References

Alaghmand, M., Shepson, P. B., Starn, T. K., Jobson, B. T., Wallace, H. W., Carroll, M. A., Bertman, S. B., Lamb, B., Edburg, S. L., Zhou, X., Apel, E., Riemer, D., Stevens, P., and Keutsch, F.: The Morning NO_x maximum in the forest atmosphere boundary layer, Atmos. Chem. Phys. Discuss., 11, 29251–29282, doi:10.5194/acpd-11-29251-2011, 2011. 27907

Ammann, C., Wolff, V., Marx, O., Brümmer, C., and Neftel, A.: Measuring the biosphere–atmosphere exchange of total reactive nitrogen by eddy covariance, Biogeosciences, 9, 4247–4261, doi:10.5194/bg-9-4247-2012, 2012. 27901

Billesbach, D. P.: Estimating uncertainties in individual eddy covariance flux measurements: a comparison of methods and a proposed new method, Agr. Forest Meteorol., 151, 394–405, doi:10.1016/j.agrformet.2010.12.001, 2011. 27903

Bonan, G.: Carbon cycle fertilizing change, Nat. Geosci., 1, 645–646, 2008. 27893

Buhr, M. P.: Solid-state light source photolytic nitrogen dioxide converter, United States Patent, 10/313827, 2007. 27896

Carroll, M. A., Bertman, S. B., and Shepson, P. B.: Overview of the Program for Research on Oxidants: PHotochemistry, Emissions, and Transport (PROPHET) summer 1998 measurements intensive, J. Geophys. Res.-Atmos., 106, 24275–24288, doi:10.1029/2001JD900189, 2001. 27896

Chaparro-Suarez, I. G., Meixner, F. X., and Kesselmeier, J.: Nitrogen dioxide (NO_2) uptake by vegetation controlled by atmospheric concentrations and plant stomatal aperture, Atmos. Environ., 45, 5742–5750, 2011. 27894

De Sousa, A. N. F.: Wet and dry deposition of water-soluble inorganic ions, in particulare reactive nitrogen species, to Haliburton Forest, Ph.D. thesis, University of Toronto, 2010. 27915

Farmer, D. K. and Cohen, R. C.: Observations of HNO_3, ΣAN, ΣPN and NO_2 fluxes: evidence for rapid HO_x chemistry within a pine forest canopy, Atmos. Chem. Phys., 8, 3899–3917, doi:10.5194/acp-8-3899-2008, 2008. 27903, 27913

Farmer, D. K., Wooldridge, P. J., and Cohen, R. C.: Application of thermal-dissociation laser induced fluorescence (TD-LIF) to measurement of HNO_3, Σalkyl nitrates, Σperoxy nitrates, and NO_2 fluxes using eddy covariance, Atmos. Chem. Phys., 6, 3471–3486, doi:10.5194/acp-6-3471-2006, 2006. 27901

Flechard, C. R., Nemitz, E., Smith, R. I., Fowler, D., Vermeulen, A. T., Bleeker, A., Erisman, J. W., Simpson, D., Zhang, L., Tang, Y. S., and Sutton, M. A.: Dry deposition of reactive

ACPD
13, 27891–27936, 2013

nitrogen to European ecosystems: a comparison of inferential models across the NitroEurope network, Atmos. Chem. Phys., 11, 2703–2728, doi:10.5194/acp-11-2703-2011, 2011. 27893

Foken, T. and Wichura, B.: Tools for quality assessment of surface-based flux measurements, Agr. Forest Meteorol., 78, 83–105, doi:10.1016/0168-1923(95)02248-1, 1996. 27900

Fowler, D., Pilegaard, K., Sutton, M. A., Ambus, P., Raivonen, M., Duyzer, J., Simpson, D., Fagerli, H., Fuzzi, S., Schjoerring, J. K., Granier, C., Neftel, A., Isaksen, I. S. A., Laj, P., Maione, M., Monks, P. S., Burkhardt, J., Daemmgen, U., Neirynck, J., Personne, E., Wichink-Kruit, R., Butterbach-Bahl, K., Flechard, C., Tuovinen, J. P., Coyle, M., Gerosa, G., Loubet, B., Altimir, N., Gruenhage, L., Ammann, C., Cieslik, S., Paoletti, E., Mikkelsen, T. N., Ro-Poulsen, H., Cellier, P., Cape, J. N., Horvath, L., Loreto, F., Niinemets, U., Palmer, P. I., Rinne, J., Misztal, P., Nemitz, E., Nilsson, D., Pryor, S., Gallagher, M. W., Vesala, T., Skiba, U., Brueggemann, N., Zechmeister-Boltenstern, S., Williams, J., O'Dowd, C., Facchini, M. C., de Leeuw, G., Flossman, A., Chaumerliac, N., and Erisman, J. W.: Atmospheric composition change: ecosystems–atmosphere interactions, Atmos. Environ., 43, 5268–5350, doi:10.1016/j.atmosenv.2009.07.068, 2009. 27917

Galloway, J. N., Aber, J. D., Erisman, J. W., Seitzinger, S. P., Howarth, R. W., Cowling, E. B., and Cosby, B. J.: The nitrogen cascade, BioScience, 53, 341–356, 2003. 27893

Ganzeveld, L. N., Lelieveld, J., Dentener, F. J., Krol, M. C., Bouwman, A. J., and Roelofs, G. J.: Global soil-biogenic NO_x emissions and the role of canopy processes, J. Geophys. Res.-Atmos., 107, 4298, doi:10.1029/2001JD001289, 2002. 27894

Gao, W., Wesely, M. L., and Lee, I. Y.: A numerical study of the effects of air chemistry on fluxes of NO, NO_2, and O_3 near the surface, J. Geophys. Res.-Atmos., 96, 18761–18769, doi:10.1029/91JD02106, 1991. 27915

Gao, W., Wesely, M. L., and Doskey, P. V.: Numerical modeling of the turbulent-diffusion and chemistry of NO_x, O_3, isoprene, and other reactive trace gases in and above a forest canopy, J. Geophys. Res.-Atmos., 98, 18339–18353, doi:10.1029/93JD01862, 1993. 27916

Hogg, A. J.: Stomatal and non-stomatal fluxes of ozone, NO_x, and NO_y to a northern mixed hardwood forest, Ph.D. thesis, University of Michigan, 2007. 27902, 27909, 27910, 27914, 27925

Holland, E. A., Braswell, B. H., Sulzman, J., and Lamarque, J. F.: Nitrogen deposition onto the United States and western Europe: synthesis of observations and models, Ecol. Appl., 15, 38–57, doi:10.1890/03-5162, 2005. 27894, 27912

ACPD
13, 27891–27936, 2013

Horii, C. V., Munger, J. W., Wofsy, S. C., Zahniser, M., Nelson, D., and McManus, J. B.: Fluxes of nitrogen oxides over a temperate deciduous forest, J. Geophys. Res.-Atmos., 109, D08305, doi:10.1029/2003jd004326, 2004. 27913, 27916

Horii, C. V., Munger, J. W., Wofsy, S. C., Zahniser, M., Nelson, D., and McManus, J. B.: Atmospheric reactive nitrogen concentration and flux budgets at a Northeastern US forest site, Agr. Forest Meteorol., 136, 159–174, 2006. 27894

Kaimal, J. C., Izumi, Y., Wyngaard, J. C., and Cote, R.: Spectral characteristics of surface-layer turbulence, Q. J. Roy. Meteor. Soc., 98, 563–589, doi:10.1002/qj.49709841707, 1972. 27906

Lee, J. D., Moller, S. J., Read, K. A., Lewis, A. C., Mendes, L., and Carpenter, L. J.: Year-round measurements of nitrogen oxides and ozone in the tropical North Atlantic marine boundary layer, J. Geophys. Res.-Atmos., 114, D21302, doi:10.1029/2009JD011878 2009. 27896, 27898

Lerdau, M. T., Munger, L. J., and Jacob, D. J.: Atmospheric chemistry – the NO_2 flux conundrum, Science, 289, 2291–2293, doi:10.1126/science.289.5488.2291, 2000. 27894

Magnani, F., Mencuccini, M., Borghetti, M., Berbigier, P., Berninger, F., Delzon, S., Grelle, A., Hari, P., Jarvis, P. G., Kolari, P., Kowalski, A. S., Lankreijer, H., Law, B. E., Lindroth, A., Loustau, D., Manca, G., Moncrieff, J. B., Rayment, M., Tedeschi, V., Valentini, R., and Grace, J.: The human footprint in the carbon cycle of temperate and boreal forests, Nature, 447, 848–850, 2007. 27893

Min, K.-E., Pusede, S. E., Browne, E. C., LaFranchi, B. W., Wooldridge, P. J., Wolfe, G. M., Harrold, S. A., Thornton, J. A., and Cohen, R. C.: Observations of atmosphere-biosphere exchange of total and speciated peroxynitrates: nitrogen fluxes and biogenic sources of peroxynitrates, Atmos. Chem. Phys., 12, 9763–9773, doi:10.5194/acp-12-9763-2012, 2012. 27913

Min, K.-E., Pusede, S. E., Browne, E. C., LaFranchi, B. W., Wooldridge, P. J., and Cohen, R. C.: Eddy covariance fluxes and vertical concentration gradient measurements of NO and NO_2 over a ponderosa pine ecosystem: observational evidence for within canopy removal of NO_x, Atmos. Chem. Phys. Discuss., 13, 12437–12484, doi:10.5194/acpd-13-12437-2013, 2013. 27916

Munger, J. W., Wofsy, S. C., Bakwin, P. S., Fan, S. M., Goulden, M. L., Daube, B. C., Goldstein, A. H., Moore, K. E., and Fitzjarrald, D. R.: Atmospheric deposition of reactive nitrogen oxides and ozone in a temperate deciduous forest and a subarctic woodland, 1. Measure-

ACPD
13, 27891–27936, 2013

ments and mechanisms, J. Geophys. Res.-Atmos., 101, 12639–12657, 1996. 27901, 27902, 27909, 27912, 27917

Munger, J. W., Fan, S. M., Bakwin, P. S., Goulden, M. L., Goldstein, A. H., Colman, A. S., and Wofsy, S. C.: Regional budgets for nitrogen oxides from continental sources: variations of rates for oxidation and deposition with season and distance from source regions, J. Geophys. Res.-Atmos., 103, 8355–8368, doi:10.1029/98JD00168, 1998. 27910, 27912, 27925

Neirynck, J., Kowalski, A. S., Carrara, A., Genouw, G., Berghmans, P., and Ceulemans, R.: Fluxes of oxidised and reduced nitrogen above a mixed coniferous forest exposed to various nitrogen emission sources, Environ. Pollut., 149, 31–43, doi:10.1016/j.envpol.2006.12.029, 2007. 27913

Papale, D., Reichstein, M., Aubinet, M., Canfora, E., Bernhofer, C., Kutsch, W., Longdoz, B., Rambal, S., Valentini, R., Vesala, T., and Yakir, D.: Towards a standardized processing of Net Ecosystem Exchange measured with eddy covariance technique: algorithms and uncertainty estimation, Biogeosciences, 3, 571–583, doi:10.5194/bg-3-571-2006, 2006. 27898

Pryor, S. C., Barthelmie, R. J., Jensen, B., Jensen, N. O., and Sorensen, L. L.: HNO_3 fluxes to a deciduous forest derived using gradient and REA methods, Atmos. Environ., 36, 5993–5999, doi:10.1016/S1352-2310(02)00765-3, 2002. 27913

Querino, C. A. S., Smeets, C. J. P. P., Vigano, I., Holzinger, R., Moura, V., Gatti, L. V., Martinewski, A., Manzi, A. O., de Araújo, A. C., and Röckmann, T.: Methane flux, vertical gradient and mixing ratio measurements in a tropical forest, Atmos. Chem. Phys., 11, 7943–7953, doi:10.5194/acp-11-7943-2011, 2011. 27906

Reidmiller, D. R., Jaffe, D. A., Fischer, E. V., and Finley, B.: Nitrogen oxides in the boundary layer and free troposphere at the Mt. Bachelor Observatory, Atmos. Chem. Phys., 10, 6043–6062, doi:10.5194/acp-10-6043-2010, 2010. 27896

Schmid, H. P., Su, H. B., Vogel, C. S., and Curtis, P. S.: Ecosystem–atmosphere exchange of carbon dioxide over a mixed hardwood forest in northern lower Michigan, J. Geophys. Res.-Atmos., 108, 4417, doi:10.1029/2002JD003011, 2003. 27896

Seok, B., Helmig, D., Ganzeveld, L., Williams, M. W., and Vogel, C. S.: Dynamics of nitrogen oxides and ozone above and within a mixed hardwood forest in northern Michigan, Atmos. Chem. Phys., 13, 7301–7320, doi:10.5194/acp-13-7301-2013, 2013. 27907

Sievering, H., Kelly, T., McConville, G., Seibold, C., and Turnipseed, A.: Nitric acid dry deposition to conifer forests: Niwot Ridge spruce-fir-pine study, Atmos. Environ., 35, 3851–3859, doi:10.1016/S1352-2310(01)00156-X, 2001. 27913

ACPD
13, 27891–27936, 2013

Smeets, C. J. P. P., Holzinger, R., Vigano, I., Goldstein, A. H., and Röckmann, T.: Eddy covariance methane measurements at a Ponderosa pine plantation in California, Atmos. Chem. Phys., 9, 8365–8375, doi:10.5194/acp-9-8365-2009, 2009. 27906

Sparks, J. P., Monson, R. K., Sparks, K. L., and Lerdau, M.: Leaf uptake of nitrogen dioxide (NO_2) in a tropical wet forest: implications for tropospheric chemistry, Oecologia, 127, 214–221, doi:10.1007/s004420000594, 2001. 27894

Sparks, J. P., Walker, J., Turnipseed, A., and Guenther, A.: Dry nitrogen deposition estimates over a forest experiencing free air CO_2 enrichment, Glob. Change Biol., 14, 768–781, doi:10.1111/j.1365-2486.2007.01526.x, 2008. 27894, 27910, 27913, 27925

Suyker, A. E. and Verma, S. B.: Eddy-correlation measurement of CO_2 flux using a closed-path sensor – theory and field-tests against an open-path sensor, Bound.-Lay. Meteorol., 64, 391–407, doi:10.1007/BF00711707, 1993. 27905

Templer, P. H., Pinder, R. W., and Goodale, C. L.: Effects of nitrogen deposition on greenhouse-gas fluxes for forests and grasslands of North America, Front Ecol. Environ., 10, 547–553, doi:10.1890/120055, 2012. 27893

Thomas, R. Q., Canham, C. D., Weathers, K. C., and Goodale, C. L.: Increased tree carbon storage in response to nitrogen deposition in the US, Nat. Geosci., 3, 13–17, doi:10.1038/NGEO721, 2010. 27893

Turnipseed, A. A., Huey, L. G., Nemitz, E., Stickel, R., Higgs, J., Tanner, D. J., Slusher, D. L., Sparks, J. P., Flocke, F., and Guenther, A.: Eddy covariance fluxes of peroxyacetyl nitrates (PANs) and NO_y to a coniferous forest, J. Geophys. Res.-Atmos., 111, D09304, doi:10.1029/2005jd006631, 2006. 27901, 27913

Venterea, R. T., Groffman, P. A., Castro, M. S., Verchot, L. V., Fernandez, I. J., and Adams, M. B.: Soil emissions of nitric oxide in two forest watersheds subjected to elevated N inputs, Forest Ecol. Manag., 196, 335–349, doi:10.1016/j.foreco.2004.03.028, 2004. 27917

Vitousek, P. M., Aber, J. D., Howarth, R. W., Likens, G. E., Matson, P. A., Schindler, D. W., Schlesinger, W. H., and Tilman, D.: Human alteration of the global nitrogen cycle: sources and consequences, Ecol. Appl., 7, 737–750, doi:10.2307/2269431, 1997. 27893

Webb, E. K., Pearman, G. I., and Leuning, R.: Correction of flux measurements for density effects due to heat and water-vapor transfer, Q. J. Roy. Meteor. Soc., 106, 85–100, doi:10.1002/qj.49710644707, 1980. 27900, 27901

Wesely, M. L. and Hicks, B. B.: A review of the current status of knowledge on dry deposition, Atmos. Environ., 34, 2261–2282, doi:10.1016/S1352-2310(99)00467-7, 2000. 27893, 27894

ACPD
13, 27891–27936, 2013

Wilczak, J. M., Oncley, S. P., and Stage, S. A.: Sonic anemometer tilt correction algorithms, Bound.-Lay. Meteorol., 99, 127–150, doi:10.1023/A:1018966204465, 2001. 27899

Williams, E. J. and Fehsenfeld, F. C.: Measurement of soil-nitrogen oxide emissions at 3 north-american ecosystems, J. Geophys. Res.-Atmos., 96, 1033–1042, doi:10.1029/90JD01903, 1991. 27917

Williams, E. J., Parrish, D. D., Buhr, M. P., Fehsenfeld, F. C., and Fall, R.: Measurement of soil nox emissions in Central Pennsylvania, J. Geophys. Res.-Atmos., 93, 9539–9546, doi:10.1029/JD093iD08p09539, 1988. 27917

Wolfe, G. M., Thornton, J. A., Yatavelli, R. L. N., McKay, M., Goldstein, A. H., LaFranchi, B., Min, K.-E., and Cohen, R. C.: Eddy covariance fluxes of acyl peroxy nitrates (PAN, PPN and MPAN) above a Ponderosa pine forest, Atmos. Chem. Phys., 9, 615–634, doi:10.5194/acp-9-615-2009, 2009. 27913

Wolff, V., Trebs, I., Foken, T., and Meixner, F. X.: Exchange of reactive nitrogen compounds: concentrations and fluxes of total ammonium and total nitrate above a spruce canopy, Biogeosciences, 7, 1729–1744, doi:10.5194/bg-7-1729-2010, 2010. 27913

Zhang, L., Brook, J. R., and Vet, R.: A revised parameterization for gaseous dry deposition in air-quality models, Atmos. Chem. Phys., 3, 2067–2082, doi:10.5194/acp-3-2067-2003, 2003. 27915, 27916

Zhang, L., Vet, R., O'Brien, J. M., Mihele, C., Liang, Z., and Wiebe, A.: Dry deposition of individual nitrogen species at eight Canadian rural sites, J. Geophys. Res.-Atmos., 114, D02301, doi:10.1029/2008JD010640, 2009. 27894, 27915

Zhang, L., Jacob, D. J., Knipping, E. M., Kumar, N., Munger, J. W., Carouge, C. C., van Donkelaar, A., Wang, Y. X., and Chen, D.: Nitrogen deposition to the United States: distribution, sources, and processes, Atmos. Chem. Phys., 12, 4539–4554, doi:10.5194/acp-12-4539-2012, 2012. 27894, 27913

ACPD
13, 27891–27936, 2013

Table 1. Average daily summertime NO_y fluxes above several North American forests measured directly by eddy covariance.

Location	Coordinates	Time Period	Average Daily Flux
Schefferville[a]	54°50′ N, 66°40′ W	Jul–Aug 1990	0.11
HFWR[b]	45°17′ N, 78°32′ W	27 Jul–6 Oct 2011	0.14
PROPHET[c]	45°33′ N, 84°42′ W	Aug 2005	0.15
PROPHET[b]	45°33′ N, 84°42′ W	24 Jul–14 Aug 2012	0.34
Harvard Forest[a]	42°32′ N, 72°11′ W	1990–1996	0.70
Duke Forest[d]	35°58′ N, 79°05′ W	11–25 Jul 2003	0.75

[a] Munger et al. (1998).
[b] Present study.
[c] Hogg (2007).
[d] Sparks et al. (2008).

ACPD
13, 27891–27936, 2013

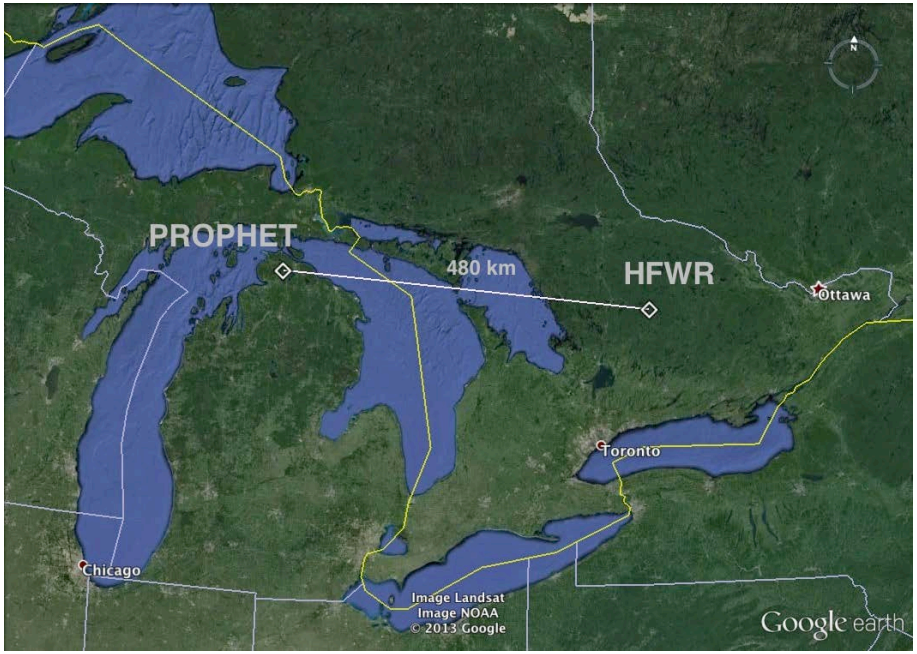

Fig. 1. Locations of PROPHET and HFWR towers.

ACPD
13, 27891–27936, 2013

Eddy covariance NO_y fluxes above two forests

J. A. Geddes and
J. G. Murphy

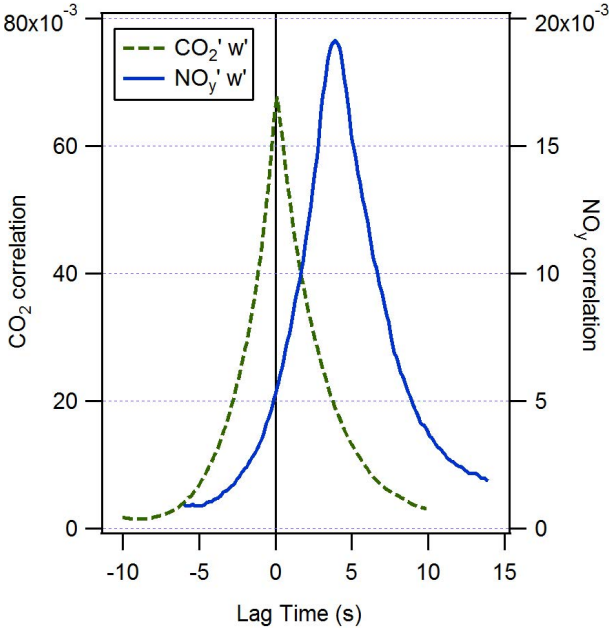

Fig. 2. Average lagged correlation plot to determine the true lag between NO_y sensor response and vertical wind (w') observations. Also shown is the lagged correlation plot for $w'CO_2'$.

ACPD
13, 27891–27936, 2013

Eddy covariance NO_y fluxes above two forests

J. A. Geddes and
J. G. Murphy

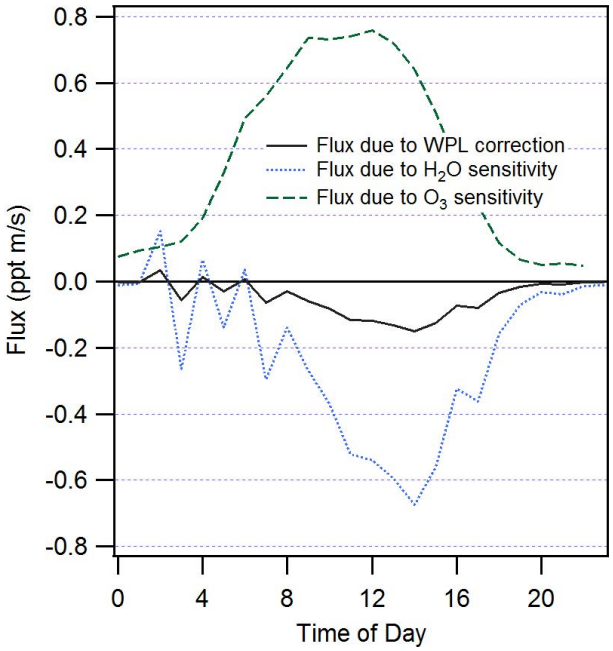

Fig. 3. Estimated flux interference terms due to water (WPL and chemiluminescent sensitivity) and ozone as a function of time of day.

ACPD
13, 27891–27936, 2013

Eddy covariance NO_y fluxes above two forests

J. A. Geddes and
J. G. Murphy

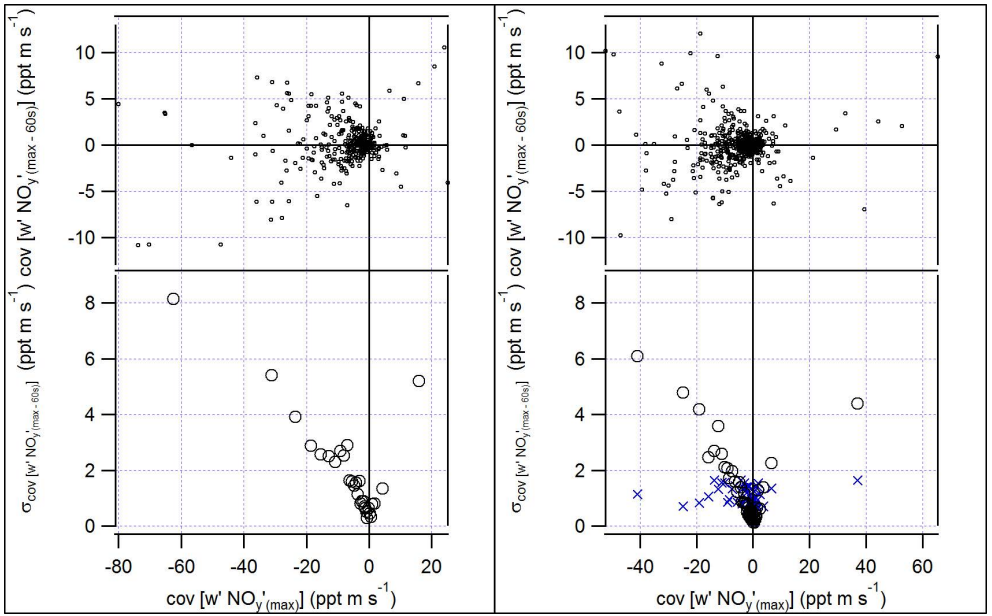

Fig. 4. Uncertainty calculated for half hour measurements of $w'NO_y'$. Top panels show the measured "zero" covariance by lagging the sensor wave by 60 s, highlighting that these observations are grouped around the zero line. The bottom panels show the standard deviation of equally sized bins of zero measurements as a function of "true" covariance at maximum covariance lag time. Results for PROPHET are shown in **(a)**, and results from HFWR are shown in **(b)**, where the "X" markers are the results from the zero-air approach.

ACPD
13, 27891–27936, 2013

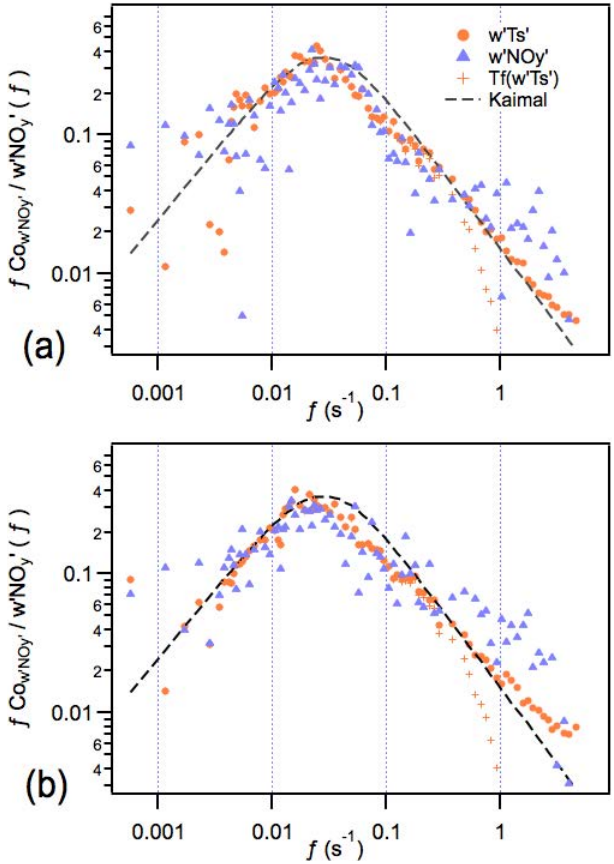

Fig. 5. Normalized cospectra of $w'NO_y'$. See text for details.

ACPD
13, 27891–27936, 2013

Eddy covariance NO_y fluxes above two forests

J. A. Geddes and
J. G. Murphy

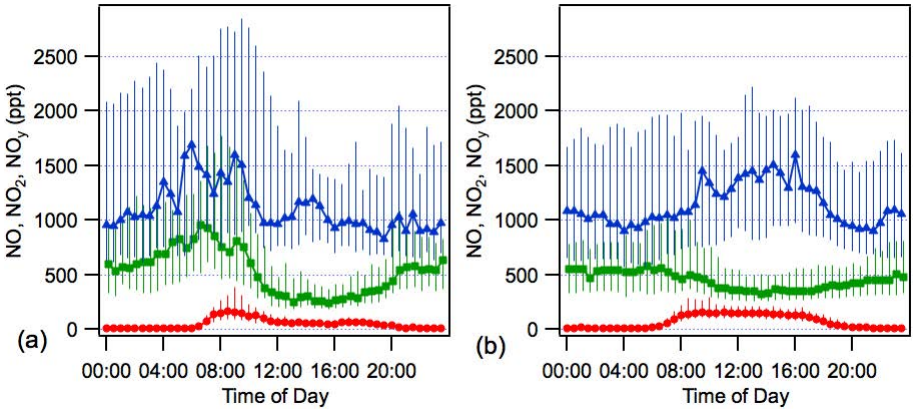

Fig. 6. Diurnal average NO (red circles), NO_2 (green squares), and NO_y (blue triangles) mixing ratios at **(a)** PROPHET and **(B)** HFWR. Line with markers indicate the median, vertical lines denote the middle 50 % distribution of the data.

ACPD
13, 27891–27936, 2013

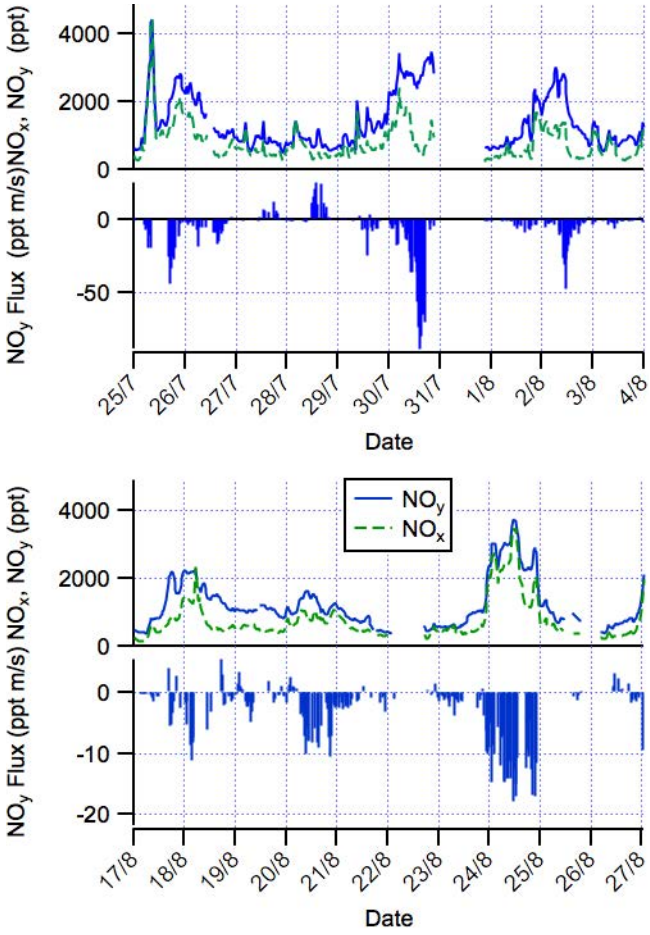

Fig. 7. Example 10 day time series for NO_x and NO_y mixing ratios and eddy covariance NO_y fluxes at **(a)** PROPHET and **(b)** HFW.

ACPD
13, 27891–27936, 2013

Eddy covariance NO_y fluxes above two forests

J. A. Geddes and
J. G. Murphy

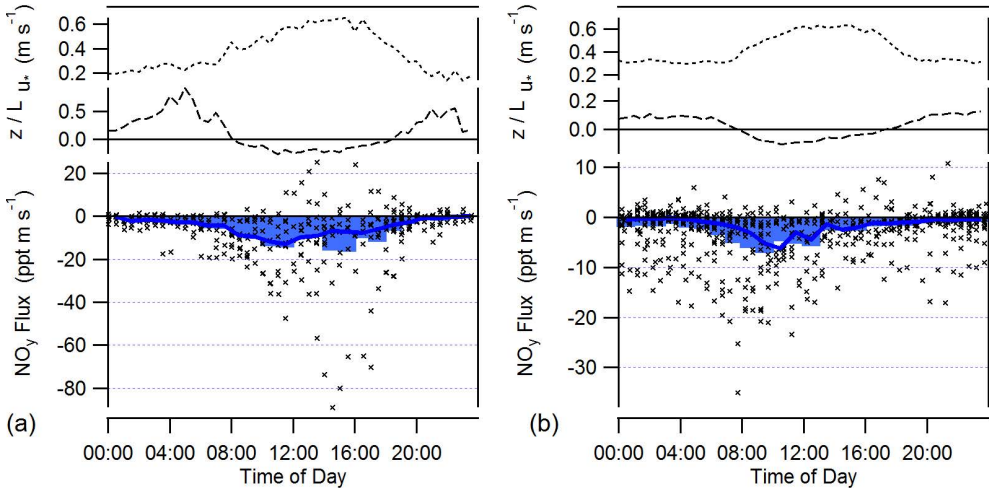

Fig. 8. Diurnal median u_*, MO z L^{-1}, and eddy covariance NO_y fluxes for **(a)** PROPHET and **(b)** HFWR. In the lower panel, bars represent the hourly mean, the solid line represents the median, and the markers represent individual observations.

ACPD
13, 27891–27936, 2013

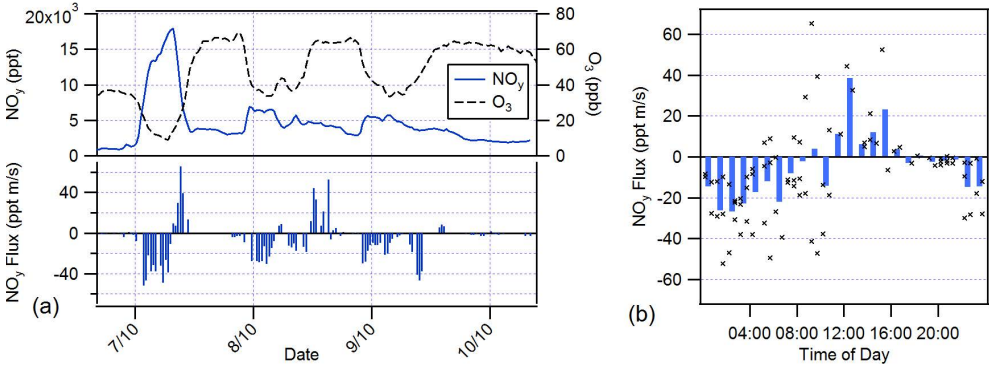

Fig. 9. (a) Mixing ratio and flux observations, and **(b)** diurnal average during the high pollution event from 7 October to 9 October 2011 at HFWR.

ACPD
13, 27891–27936, 2013

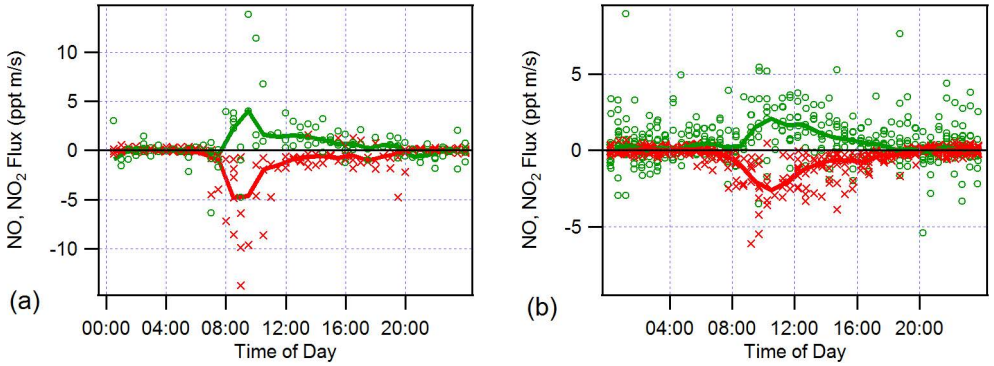

Fig. 10. Diurnal plot of NO (red, crosses) and NO_2 (green open circles) fluxes observed at **(a)** PROPHET and **(b)** HFWR. Solid lines indicate hourly median.

ACPD
13, 27891–27936, 2013

Eddy covariance NO_y fluxes above two forests

J. A. Geddes and
J. G. Murphy

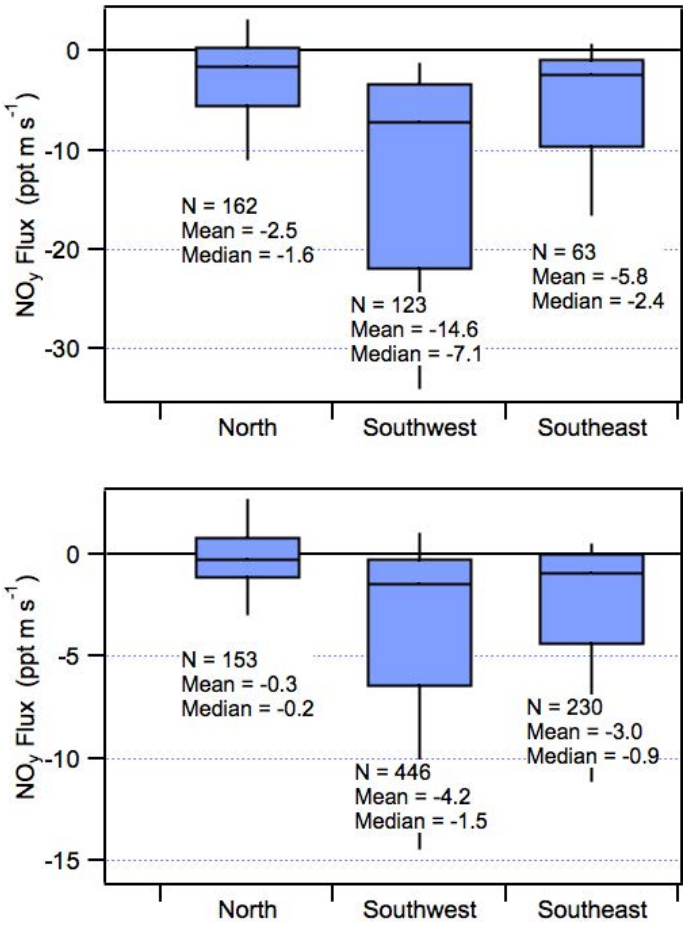

Fig. 11. Average NO_y flux observations ($ppt\,m\,s^{-1}$) organized by observed wind direction at **(a)** PROPHET and **(b)** HFWR.

ACPD
13, 27891–27936, 2013